Bulletin of the JSME Vol.10, No.1, 2015
Journal of Thermal Science and Technology

Effects of electrode configurations on the combustion characteristics of premixed methane-air flames

Jianfeng FANG*, Xiaomin WU*,**, Hao DUAN*, Chao LI* and Zhongquan GAO*
*Institute of Internal Combustion Engine, Xi'an Jiaotong University, Xi'an, 710049, China
E-mail: xmwu@mail.xjtu.edu.cn
**Shaanxi University of Technology, Hanzhong, 723001, China

Received 26 November 2014

Abstract
The present paper reported the effects of electric fields produced by the mesh, ring and needle electrodes on outwardly propagating premixed flames in a constant chamber. The input voltages were 0 kV, -5 kV, -10 kV, -12 kV, and the excess air ratios of methane-air mixture were 0.8, 1.0 and 1.2, respectively. The electric field distributions developed by the three electrode configurations all affected the flame propagation in the horizontal direction rather than in the vertical direction. The electric field strength for the mesh electrode in the region between the high-voltage electrodes was the largest, and that for the ring and needle electrode decreased in turn. Under the application of the electric field, the flame front was stretched remarkably and the flame speed was accelerated significantly as the input voltage increased. For the three electrode geometries, the increase of the flame speed for the mesh electrode was the largest, followed by that for the ring and needle electrodes. For various excess air ratios, the increase of the flame speed at lean mixture was the largest, that at rich mixture the less large and that at stoichiometric mixture the smallest. By analyzing the effects of the three electrode geometries on pressure data, it was seen that the applied electric field could markedly enhance the combustion pressure growing up, and the timing of the peak pressure was advanced with the increase of the input voltage. The promotion effect on the combustion is most pronounced for the mesh electrode, while that for the ring and needle electrodes decreased in turn. For the various excess air ratios, the electric field most significantly enhanced the combustion pressure growing up at lean mixture.

Key words: Electric field distribution, Ionic wind effect, Spherical flame, Propagation speed, Combustion pressure

1. Introduction

It is well known that the radical ions, such as CH_3^+, H_3O^+, $C_3H_3^+$, CHO^+ and electrons, are found during the combustion using hydrocarbon as fuel. So the application of an electric field can strongly affect the flame front behavior and combustion characteristics. In recent years, considerable efforts have been directed to the study of flame and electric field interaction and its effects on the combustion process. In those studies, flames of various types such as Bunsen flame (Wisman, et al., 2007, Sakhrieh, et al., 2005, Kim, et al., 2011, Altendorfner, et al., 2011, Calcote, et al., 1951), jet flame (Lee, et al., 2005, Kim, et al., 2010), flat flame (Kiyotaka, et al., 2009), tribrachial flow flame (Volkov, et al., 2013), etc. were used, and direct-current (DC) (Papac, et al., 2008, van den Boom, et al., 2009, Katzer, et al., 2001, Jing, et al., 2000, Memdouh, et al., 2010, Shinichi, et al., 2008, Eugene, et al., 2008, Marcum, et al., 2005) and alternating-current (AC) (Ryu, et al., 2010, Xie, et al., 1993, Won, et al., 2007, Won, et al., 2008, Zake, et al., 2001, Min, et al., 2012) electric fields were presented. For example, Calcote observed that by applying a longitudinal electric field directed towards the burner, the stability limit of a flame of n-butane and air on a Bunsen burner could be extended significantly. They attributed the effect to an ionic wind induced by the interaction of the electric field with chemi-ions present in the flame (Calcote, et al., 1951). S.D. Marcum conducted experiments on electric field induced flame speed modification by the application of pulsed DC electric field and reported that the flame speed of premixed propane-air flame could be increased substantially due to the flame front wrinkling and the increased reaction area

Paper No.14-00502
[DOI: 10.1299/jtst.2015jtst0020]

(Marcum, et al., 2005). Min investigated the stabilization of laminar premixed Bunsen flames by applying DC and low frequency AC electric fields. They used the bi-ionic wind effects to explain the fact that the AC electric field could have minimal influence on flame stabilization (Min, et al., 2012). Through electrically enhanced combustion, stabilizing flames (Kim, et al., 2005, Memdouh, et al., 2010, Min, et al., 2012), reducing carbon formation (Won, et al., 2007) and increasing flame velocity (van den Boom, et al., 2009, Shinichi, et al., 2008, Eugene, et al., 2008) are among the main effects that have been observed.

Up to now, the studies of the effects of electric field on combustion have been focused on the stable flames such as Bunsen flame and candle-typed flame (Jing, et al., 2000), etc, but there has been little literature reporting the effects of electric field on the outwardly propagating spherical flame. In fact, the combustion of a homogeneous mixture in a constant volume vessel can easily be used to determine the flame laminar burning velocity owing to its simple and well-proven combustion geometry. The laminar burning velocity is fundamentally important in regard to developing and justifying the chemical kinetic mechanisms and for predicting the performance of combustion systems (Huang, et al., 2007, Lamoureux, et al., 2003, Guo, et al., 2009). Recently, Cha investigated the premixed combustion under AC electric field in a constant volume chamber and reported that the electric field could induce cracked structure formation on flame surface and increase the flame propagation velocity whereas the combustion peak pressure and burning rate changed little (Min et al., 2012). Meng studied the effects of DC electric field on the combustion characteristics of the spherically expanding flames and reported that the flame laminar burning speed was increased and the overall combustion duration was shortened under the electric field. In addition, the peak pressure and rate of pressure rise at lean mixture were increased with the increase of the input voltage (Meng, et al., 2012). To figure out the interaction of the electric field with the outwardly propagating spherical flame, there are still many problems that call for further investigation, especially from the perspective of electric field distribution. Under the same input voltage, different electrode structures may result in substantially different electric field distributions and produce different effects on combustion process. The objective of this paper is to look into the effects of different electrode configurations on the combustion characteristics of spherically expanding premixed methane-air flame. In the experiment, electrode configurations of three types at different input voltages were used to create electric fields across the flame. Premixed combustion characteristics were examined by visualizing the combustion process and measuring the combustion pressure. This study is expected to provide more information about effects of the electric field on combustion characteristics.

2 Experimental section

The experimental system setup, as shown in Figure 1, consists of a constant volume combustion chamber and the systems for ignition control, fuel supply, electric field generation, data acquisition and high-speed schlieren photography. The combustion chamber is a cylinder type with an inner diameter of 130 mm and a length of 130 mm. An insulating bush made of the polytetrafluoroethylene (PTFE) with an inner diameter of 115 mm, a thickness of 7.5 mm and a length of 130 mm is installed inside the combustion chamber. Two quartz windows with a 145 mm diameter are mounted on two sides of the bomb to allow optical accessibility. The ignition electrodes are located in the vertical direction along the bomb centerline and are surrounded by the PTFE to insulate the electrics. The high-voltage electrodes applying an electric field inside the combustion chamber are connected to a DC high-voltage power supply

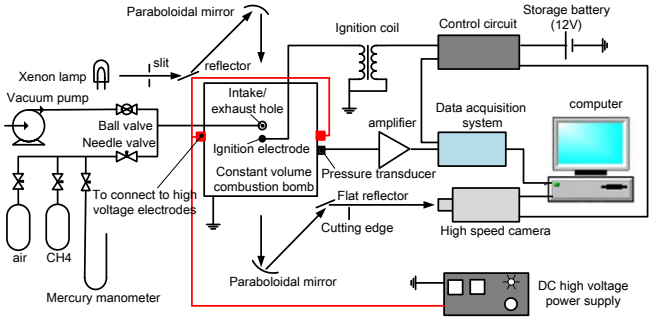

Fig. 1 Schematic of experimental system

(Weisiman DEL30N45) with the output range between 0 kV to -30 kV. In the experiment, a high-speed digital camera (HG-100K) operating at 10,000 frames per second is used to take photos of the flames during the flame propagation.

[DOI: 10.1299/jtst.2015jtst0020]

The combustion pressure is recorded by a piezo-electric kistler absolute pressure transducer with an accuracy of 0.01kPa. Methane and air are supplied into the chamber through the inlet valve according to the given excess air ratio λ (the inverse of equivalence ratio). Five minutes are waited before starting the ignition to ensure the homogeneity of the methane-air mixture.

Three different high-voltage electrode configurations are employed to generate electric fields across the flames. In the first configuration, referred to as "needle electrode", a pair of opposite stainless steel straight needles with a diameter of 4 mm are located horizontally along the bomb centerline, 35 mm away from the bomb center, respectively. In the second configuration, referred to as "mesh electrode", two stainless steel plates (with a diameter of 60 mm and a thickness of 5 mm) are located at the tips of the two needle electrodes, respectively, with a 70 mm gap between the two plates. To avoid perturbing the burnt gas development, the plate is made with a square mesh with a size of 8.5×8.5 mm and a 0.8 mm-wide mesh wire. The third configuration, referred to as "ring electrode", is a stainless steel circular ring with the inner and outer diameters being 70 mm and 80 mm, respectively, and a thickness of 5 mm. It is mounted in the vertical cross section along the bomb centerline connected to the two needle electrodes. The detailed sizes of the three electrode geometries are given in Fig. 2. In the experiment, four electric voltages (0, -5, -10, -12 kV) are supplied by the high voltage power supply. Figure 3 shows the schematic diagram of the three combustion chamber

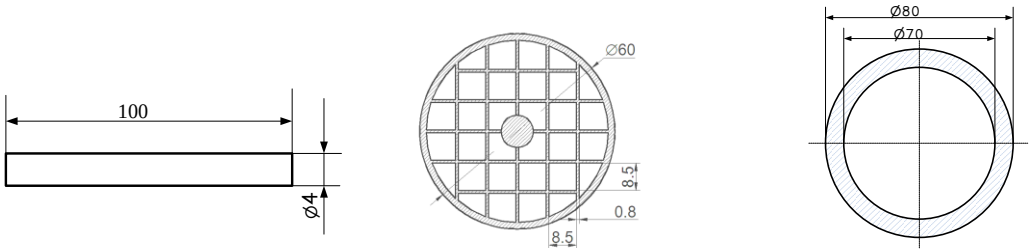

a) Needle electrode b) Mesh electrode c) Ring electrode

Fig. 2 Configurations of three different high-electrodes

configurations with their corresponding high-voltage electrodes. A homogeneous methane-air mixture is supplied at three excess air ratios of 0.8, 1.0 and 1.2, and ignited in the combustion chamber at room temperature and atmospheric pressure. Each experiment is repeated at least 3 times under the same condition, and excellent repeatability is achieved.

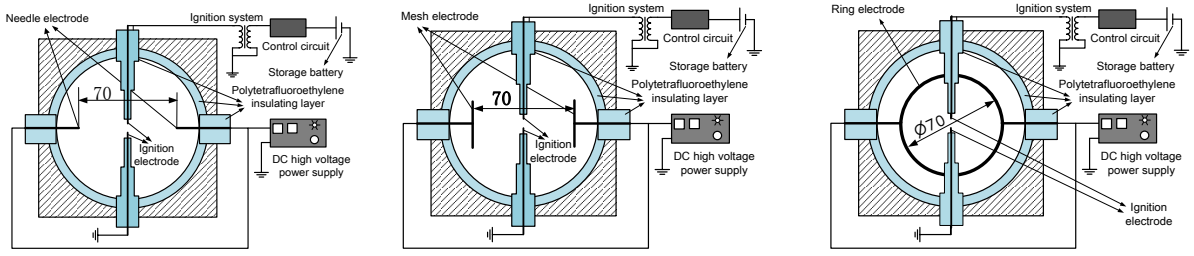

a) Needle electrode b) Mesh electrode c) Ring electrode

Fig. 3 Schematic diagram of the combustion chamber structure with each of three high-voltage electrode geometries

3 Results and discussion

3.1 Electric field distributions

In the experiment, the spatial electric field distributions produced by the three different electrode configurations at various input voltages are simulated using ANSYS 13.0. For simplicity, Figure 4 only shows the electric field distributions in the vertical cross section along the bomb centerline at an input voltage of -12 kV.

It can be seen in Fig. 4 that the electric fields generated by the three electrode geometries are all typically non-uniform and their spatial distributions are all symmetrical. For any electrode, the electric field strengths in the vicinity of both the ignition electrodes and the high-voltage electrodes change relatively largely whereas the values in the middle region between them are relatively uniform. In the meantime, the direction of the electric field line mostly points horizontally to the high-voltage electrodes from the vertical bomb centerline and the bomb circumference. Figure 5 shows the values of electric field strength along the horizontal centerline between the high-voltage electrodes for the three electrode geometries at -12 kV. For any kind of electrode, the electric field strength of each position (E_i) can be obtained from Fig. 5, and the mean value of the electric field strength (E_u) is defined as the ratio of the sum of E_i

[DOI: 10.1299/jtst.2015jtst0020]

to the number of the available electric field strength position (n). It is found that E_u for the mesh electrode is about 2.94×10^5 V/m (4.62×10^5 V/m max. 0.72×10^5 V/m min.), and the maximum and minimum values are distributed in the vicinity of the ignition electrodes. E_u for the ring electrode is about 2.46×10^5 V/m (6.1×10^5 V/m max. 2.1×10^5 V/m min.), whereas the maximum and minimum values are located in the vicinity of the ignition electrodes and the region

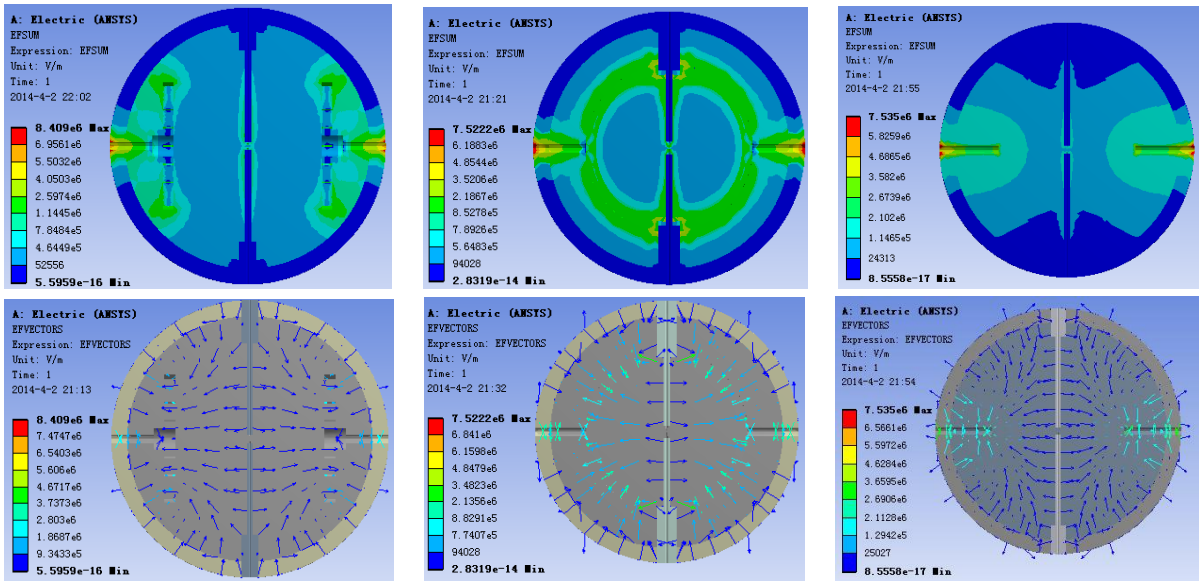

(a) Mesh electrode (b) Ring electrode (c) Needle electrode

Fig. 4 Electric field distributions for the three electrode geometries at -12kV

about 12 mm away from the bomb center, respectively. As for the needle electrode, the electric field strength almost monotonously increases from 0.14×10^5 V/m (located in the ignition electrodes) to 4.00×10^5 V/m (located in the high-voltage electrodes), with E_u being about 1.05×10^5 V/m. In short, in the region between the two high-voltage electrodes, the electric field strength for the mesh electrode is relatively uniform, and its mean value is the strongest

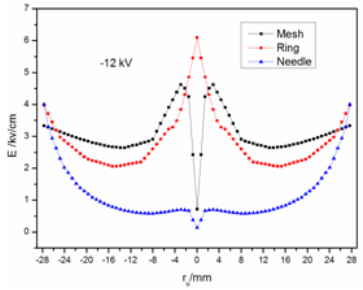

Fig. 5 The electric field strength versus the horizontal distance for the three electrode geometries at -12 kV

among the three electrode geometries. While the electric field strengths for the ring and needle electrodes change relatively large in the same range, and their mean values decrease one after another. Table 1 shows E_u between the high-voltage electrodes for the three electrode geometries at various input voltages. It can be seen that the magnitudes of the electric field strength for the three electrode geometries are proportional to the input applied voltages, and their change trends under various input voltages are in substantially consistent.

Table 1 The mean value of the electric field strength E_u for the three electrode geometries at various input voltage (A—mesh, B—ring, B—needle)

U [kV]	-5	-10	-12
E_u for A [V/m] $\times10^5$	1.23	2.45	2.94
E_u for B [V/m] $\times10^5$	1.03	2.05	2.46
E_u for C [V/m] $\times10^5$	0.43	0.88	1.05

3.2 Influence of electrode configurations on the flame shape

Figure 6 illustrates the flame propagation processes at an excess air ratio of 1.0 under the electric fields generated by the three types of electrode configurations. The input voltage and the elapsed time after the ignition are correspondingly tabulated beside the relevant flame images. For any type of electrode at an input voltage of 0 kV, i.e.,

[DOI: 10.1299/jtst.2015jtst0020]

in the absence of electric field, the flame front is almost spherical in shape and propagates evenly in both horizontal and vertical direction. When the input voltage is -5 kV, the flame propagation in the electric field direction is slightly stretched, whereas the flame front basically remains spherical in shape, and the flame surface almost keeps smooth during the process of the flame development. While, when the input voltage increases to -10 kV, or -12 kV, the flame propagation in the horizontal direction is enhanced substantially, and the flame shape is changed drastically. In the region of the high-voltage electrodes, there are intense disturbances and distortions in the horizontal flame front, and the wrinkles appear on the flame area. These results suggest that the electric field generated by any electrode geometry might affect the flame propagation from a low input voltage, and this effect increases gradually as the input voltage increases. However, it can be seen that there is an apparent discrepancies between the changes in the flame shape under the three electrode configurations at high input voltages. For the mesh electrode, the horizontal flame front is lengthened significantly and propagates evenly both leftward and rightward, whereas either of the downward and

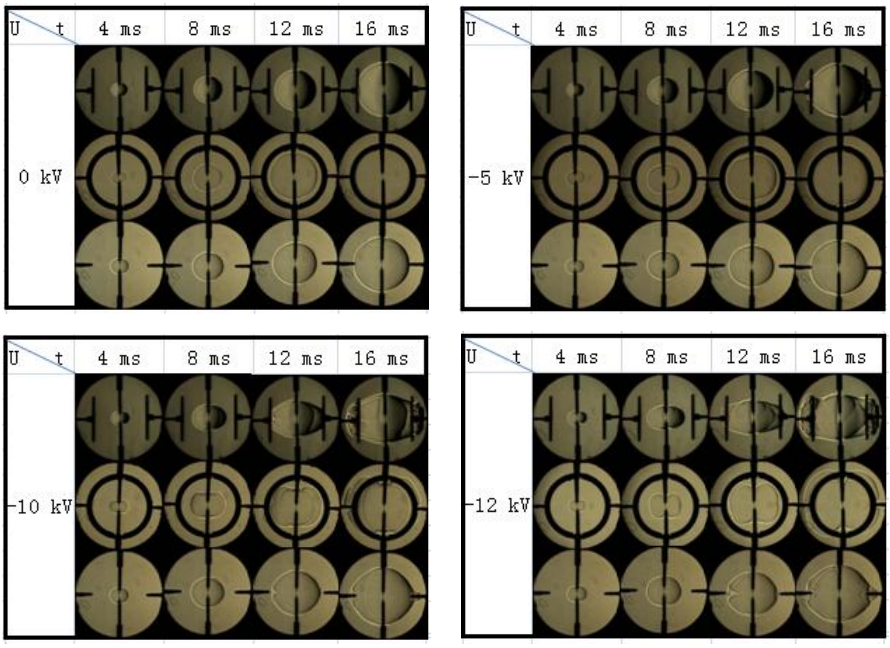

Fig. 6 Images of flame propagation process at λ= 1.0 for the three different electrode geometries

upward flame front propagations can hardly be regarded as affected, thus resulting in an elliptically shaped flame front. For the ring electrode, both the horizontal and vertical flame propagations are all stretched whereas the former propagates a lot faster than the latter, thus forming a cylindrically shaped flame front. However, in the case of the needle electrode, the flame shape change little and almost retains its previous spherical flame front.

3.3 Influence of electrode configurations on flame propagation velocity

As can be seen in Figure 6, the flame front propagation can change remarkably under the influence of the three electrode geometries. However, for every electrode, the horizontal flame front propagation is enhanced remarkably whereas the vertical flame propagation changes little. For this reason, we investigate the laminar flame velocity in the

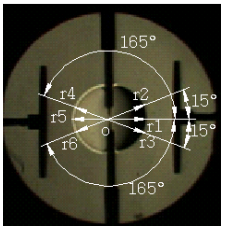

Fig. 7 Data obtained from a flame image

horizontal direction to make clear the influence of the three electrode geometries on flame propagation. The stretched flame propagation velocity, S_n, reflecting the flame moving speed relative to the motionless combustion wall, is derived from the flame propagation radius versus time (Guo, et al., 2009), $S_n=dr_u/dt$, where, r_u is the horizontal flame radius and t is the elapsed time after spark ignition. In this paper, for accurate calculation of the stretched flame propagation speed,

[DOI: 10.1299/jtst.2015jtst0020]

r_u is defined as the mean value of various flame radiuses from the ignition center to the flame front at set polar angles of 0 °, ±15 °, ±165 ° and 180 °, respectively, as shown in Fig. 7. Previous studies report that the ignition energy has an important effect on the flame propagation in its initial stage, but the influence would disappears when the flame radius is larger than about 5 mm (Hu, et al., 2009). In addition, in order to avoid the influence of wall and pressure in the combustion chamber (when the pressure rise rate is less than 1.0%), the flame radius is limited to 25 mm (Huang, et al., 2007, Lamoureux, et al., 2003). The data in this study are those of the flame radiuses from 5 mm to 25 mm.

Figure 8 shows the variations of flame radius versus the time under the three electrode geometries in the case of stoichiometric mixture. The input voltages are 0 kV, -5 kV, -10 kV and -12 kV, respectively. For an input voltage of 0 kV, the flame radius increases almost linearly with time. When an electric field generated by any electrode is applied,

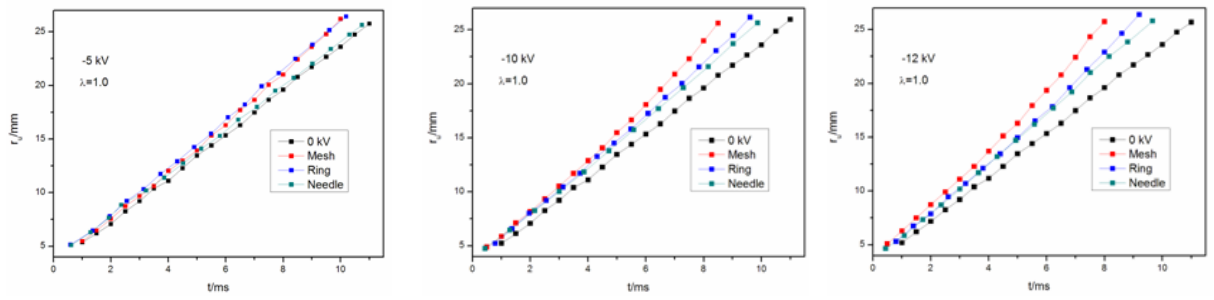

Fig. 8 Flame radius versus combustion time at various applied voltages

the flame radius at a given time is larger than that without electric field. This indicates that the electric field can enhance flame propagation. Additionally, the higher the input voltage is, the faster the flame propagates. For the three electrode geometries, the increase in the flame propagation for the mesh electrode is the fastest, that for the ring electrode the less fast and that for the needle electrode the slowest. For example, at the applied voltage of -12 kV, when r_u increases to 25 mm, the corresponding times are 7.5 ms, 8.8 ms and 9.2 ms for the mesh, ring and needle electrodes, which are advanced by 28.6%, 16.2%, and 12.4%, respectively, compared to that when no voltage is applied.

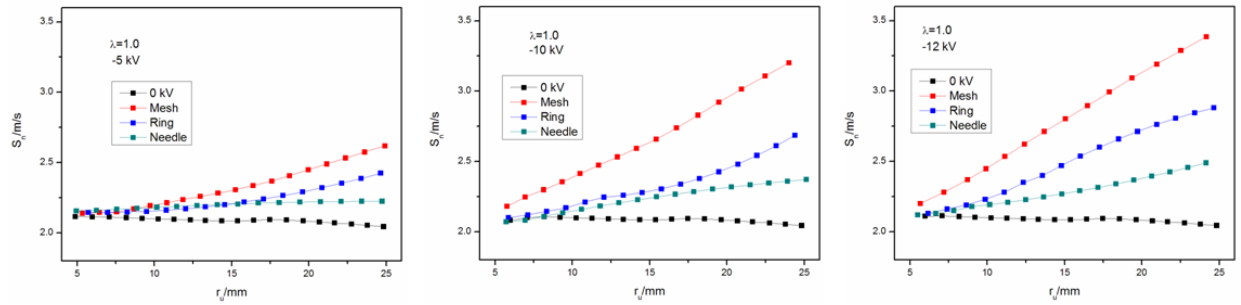

Fig. 9 Stretched flame propagation velocity versus flame radius at different applied voltages

Figure 9 illustrates the relationship between the stretched flame propagation velocity S_n and the flame radius r_u for the stoichiometric mixture. Under the influence of the electric field, the flame velocity S_n increases rapidly compared with the case without electric fields, and the effects enhance when the input voltage increases. Additionally, the influence of electric field on S_n increases with the flame propagation. For the three electrode geometries, S_n for the mesh electrode is the biggest, followed by that for the ring and needle electrodes. For example, at the input voltage of -12 kV, the maximum values of S_n are 3.43, 2.90, 2.51 m/s for the mesh, ring and needle electrodes, and are advanced by 67.3%, 41.5% and 22.5%, respectively, compared to the case without electric field.

Table 2 Average flame propagation velocity S_m for the three electrode geometries (A—mesh, B—ring, C—needle)

λ	0.8				1.0				1.2			
U [kV]	0	-5	-10	-12	0	-5	-10	-12	0	-5	-10	-12
S_m for A [m/s]	1.24	1.53	1.86	1.92	2.06	2.34	2.69	2.78	1.21	1.54	1.89	2.05
S_m for B [m/s]	1.24	1.49	1.76	1.84	2.06	2.26	2.43	2.58	1.21	1.46	1.75	1.91
S_m for C [m/s]	1.24	1.38	1.53	1.62	2.06	2.10	2.24	2.32	1.21	1.37	1.52	1.68

To compare the effects of the three electrode geometries on the flame propagation speed at various excess air ratios, table 2 shows the average flame propagation velocity S_m at excess air ratios of 0.8, 1.0 and 1.2 for the three

[DOI: 10.1299/jtst.2015jtst0020]

electrode geometries. S_m is calculated using $S_m=(r_2-r_1)/(t_2-t_1)$, where, r_1=5 mm, r_2=25 mm, t_1 and t_2 is the time when the flame radius increases to r_1 and r_2, respectively. Without the applied voltage, S_m presents its maximum value at the stoichiometric mixture, while rich and lean mixtures may decrease this value progressively. When the electric field is applied to the mixture at any excess air rate, S_m increases steadily with the increase of the input voltage. In the case of the three electrode geometries, S_m for the mesh electrode is the biggest and becomes less big for the ring and needle electrodes progressively. Table 3 shows the increase rate of S_m at various excess air ratios for the three electrode geometries. The increase rate of S_m is defined as follows: $\Delta S_m = \frac{S_m - S_{m0}}{S_{m0}} * 100\%$, where S_m and S_{m0} represent the average flame propagation velocity for a specific electrode at the voltage of u and 0 kV, respectively. For the three electrode geometries, ΔS_m for the mesh electrode is the largest, followed by that for the ring electrode and that for the needle electrode progressively. For example, at input voltage of -12 kV and lean mixture, ΔS_m for the mesh is 69%, which is higher than the ring and the needle electrode by 11% and 30%, respectively. For various excess air ratios, ΔS_m at lean mixture is the largest, that at rich mixtures less large and that at stoichiometric mixture the smallest. It is found that, for the mesh electrode at -12 kV, ΔS_m at lean mixture is 69%, which is higher than rich mixture and stoichiometric mixture by 14% and 34%, respectively.

Table 3 The increase rate of average flame propagation velocity ΔS_m for the three electrode geometries (A—mesh, B—ring, C—needle)

λ	0.8			1.0			1.2		
U [kV]	-5	-10	-12	-5	-10	-12	-5	-10	-12
ΔS_m for A [%]	23	50	55	14	31	35	27	56	69
ΔS_m for B [%]	20	42	48	10	18	25	21	45	58
ΔS_m for C [%]	11	23	31	2	9	13	13	26	39

The increase of the flame propagation speed under the three electrode geometries can mainly be ascribed to the ionic wind effects, i.e., a bulk flow movement due to electric-field-induced directional collisions of ions and neutral molecules in hydrocarbon flames (Katzer, et al., 2001, Jing, et al., 2000, Meng, et al., 2012). It is accepted that the positive ions such as H_3O^+, $C_2H_4^+$ and CHO^+ formed in the flame contribute more to the ion-molecule collision because of their abundance and greater mass than electrons (Min, et al., 2012). The ionic wind effect per unit time, which increases with electric field intensity and particle number density, generates the momentum transfer of positive ions and accelerate the neutral molecules with which the ions collide. As a result of these ion-neutral collisions within the flame front, the flame propagation will speed up in the electric field direction, and the increase is more obvious in the case of the high electric field intensity. It can be seen from Fig. 3 that the electric fields between the two high-voltage electrodes developed by the three electrode configurations all point to the high-voltage electrodes from the vertical bomb centerline, which indicates that they affect flame propagation in the horizontal direction rather than in the vertical direction. As a result, the horizontal flame propagation velocity is remarkably accelerated due to the strong ionic wind effect. In the process of the flames develop at the high input voltage, the flames collide with and pass through the electrodes with more rapid speed. So there are intense disturbances and distortions in the flame front, and the wrinkles appear on the flame area in the region of electrode. In addition, as shown in Fig. 4, the electric field for the mesh electrode is the largest, that for the ring electrode the second largest and that for the needle electrode the third largest. As a consequence, the ionic wind effect produced by the mesh electrode on the flame propagation is most pronounced whereas that produced by the ring and needle electrodes lessens progressively. These effects result in the increase of the flame speed for the mesh electrode is the biggest whereas such increases for the ring and needle electrodes becomes smaller progressively.

From tables 2 and 3, it can be found that the enhancement effect of the electric field on the flame velocity at lean mixture is the largest whereas that at the rich and stoichiometric mixture becomes smaller progressively. This result could be explained by the fact that the ionic wind effect on the flame propagation is closely related to the flame velocity itself. It is assumed that the concentrations of positive ions produced in the methane-air flame do not change significantly when the excess air ratio changes (Goodings, et al., 1977), so the same electric field distribution might produce similar enhancement effect on the flame propagation at various excess air ratios per unit time. If the flame speed itself is slow, the flame propagation within a certain distance may take more time, and this may lengthen duration of the electric field affecting the combustion process. Thus, the number density of accelerated neutral molecules that

[DOI: 10.1299/jtst.2015jtst0020]

collide with the positive ions and gain momentum from them can be increased when the available time is lengthened. This will enhance significantly the ionic wind effect on the flame propagation. In this paper, we can perform simplified calculation on the question. Based on the experimental findings of Goodings, the positive ion mole fraction in the methane flame is between 1.3 and 4.0 $\times 10^{10}$ cm^{-3} (Goodings, et al., 1979), and the ratio of number densities of neutrals to positive ions is of the order of 2×10^{8}. Thus, the number density of neutral molecules can be assumed to be about 5×10^{18} cm^{-3}. In the studies on the ionic wind effect, it has been proposed that there exists a collision response time in inducing the ionic wind effect, and its value is of the order of 10 ms (Min, et al., 2012). The experimental collision response time could be about 12 ms depending on the test condition. For the mesh electrode without electric field, the time that the flame spends to propagate in the range r_u of 5 mm－25 mm is 9.7 ms, 16.1 ms and 16.6 ms at the mixtures of λ=1.0, 0.8 and 1.2, respectively. According to the theory of ionic wind shown in Appendix A, under the electric field, the corresponding increases of mole fraction of the neutral molecules that collide with the positive ions during the period are about 2.57×10^{18}, 3.36×10^{18} and 3.39×10^{18} cm^{-3}, respectively. The increase of the number density of the accelerated neutral molecules for λ=1.2 is the largest whereas that for λ=0.8 and 1.0 becomes smaller progressively. This result causes the corresponding increase of the flame speed at various excess air ratios.

3.4 Influence of electrode configurations on the combustion pressure variation

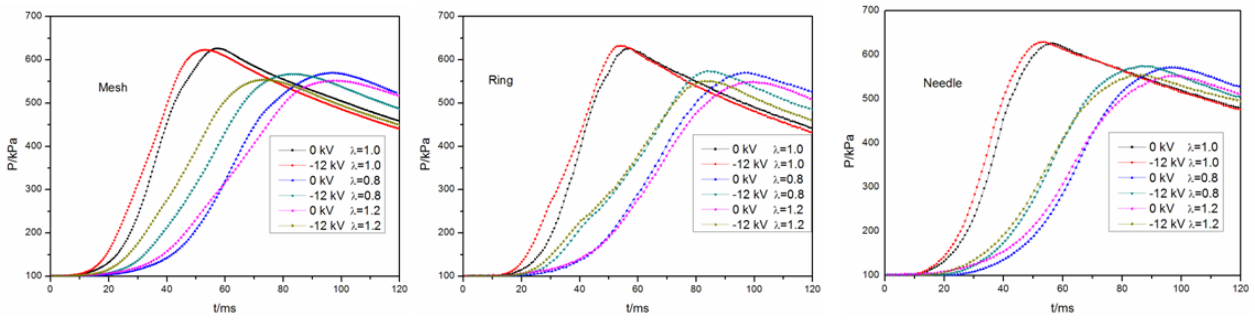

Fig.10 The combustion pressure records under the three electrode geometries

Figure 10 shows the combustion pressure records at λ=1.0, 0.8, and 1.2. The results are for the application of the three electrode configurations at input voltage of 0 kV and -12 kV. When the electric field is applied, the combustion pressure increases rapidly in the initial stage of combustion and is higher than the case without electric field. Moreover, the timing of peak pressure is advanced with the increase of the input voltage, while the peak pressure doesn't change largely for any electrode geometry. Table 4 shows the timings of peak pressure (t_p) at λ= 0.8, 1.0, 1.2 and their increase rates (Δt_p) compared to that without electric field. For the combustion at each excess air ratio without electric field, t_p is almost equal. When the electric field is applied, the mesh electrode shows the most significant advancement of t_p, followed by the ring and the needle electrode in turn. For various excess air ratios, Δt_p at lean mixture is the largest, that at rich mixtures less large and that at stoichiometric mixture the smallest. For example, in the

Table 4 The timing of peak pressure (t_p) and its increase rate (Δt_p) for the three electrode geometries

		Mesh electrodes		Ring electrodes		Needle electrodes	
λ	U(kV)	t_p(ms)	Δt_p(%)	t_p(ms)	Δt_p(%)	t_p(ms)	Δt_p(%)
0.8	0	96.8	0	97.1	0	96.5	0
	-5	89.7	-7.3	91.0	-6.3	93.2	-3.4
	-10	84.5	-12.7	87.1	-10.3	90.3	-6.4
	-12	81.6	-15.7	83.9	-13.6	86.8	-10.1
1.0	0	57.4	0	57.6	0	56.2	0
	-5	54.1	-5.8	55.8	-3.1	54.6	-2.9
	-10	53.7	-6.5	54.6	-5.2	53.8	-4.3
	-12	52.9	-7.8	53.3	-7.5	53.1	-5.5
1.2	0	97.7	0	98.1	0	97.5	0
	-5	88.2	-9.7	92.8	-5.4	93.6	-4.0
	-10	80.2	-17.9	86.3	-11.8	88.9	-8.8
	-12	75.1	-23.1	82.8	-15.6	85.7	-12.1

[DOI: 10.1299/jtst.2015jtst0020]

case of lean mixture and applied voltage of -12 kV, t_p is advanced by almost 23.1%, 15.6% and 12.1%, for the mesh, ring and needle electrodes, respectively, compared with the case without electric fields.

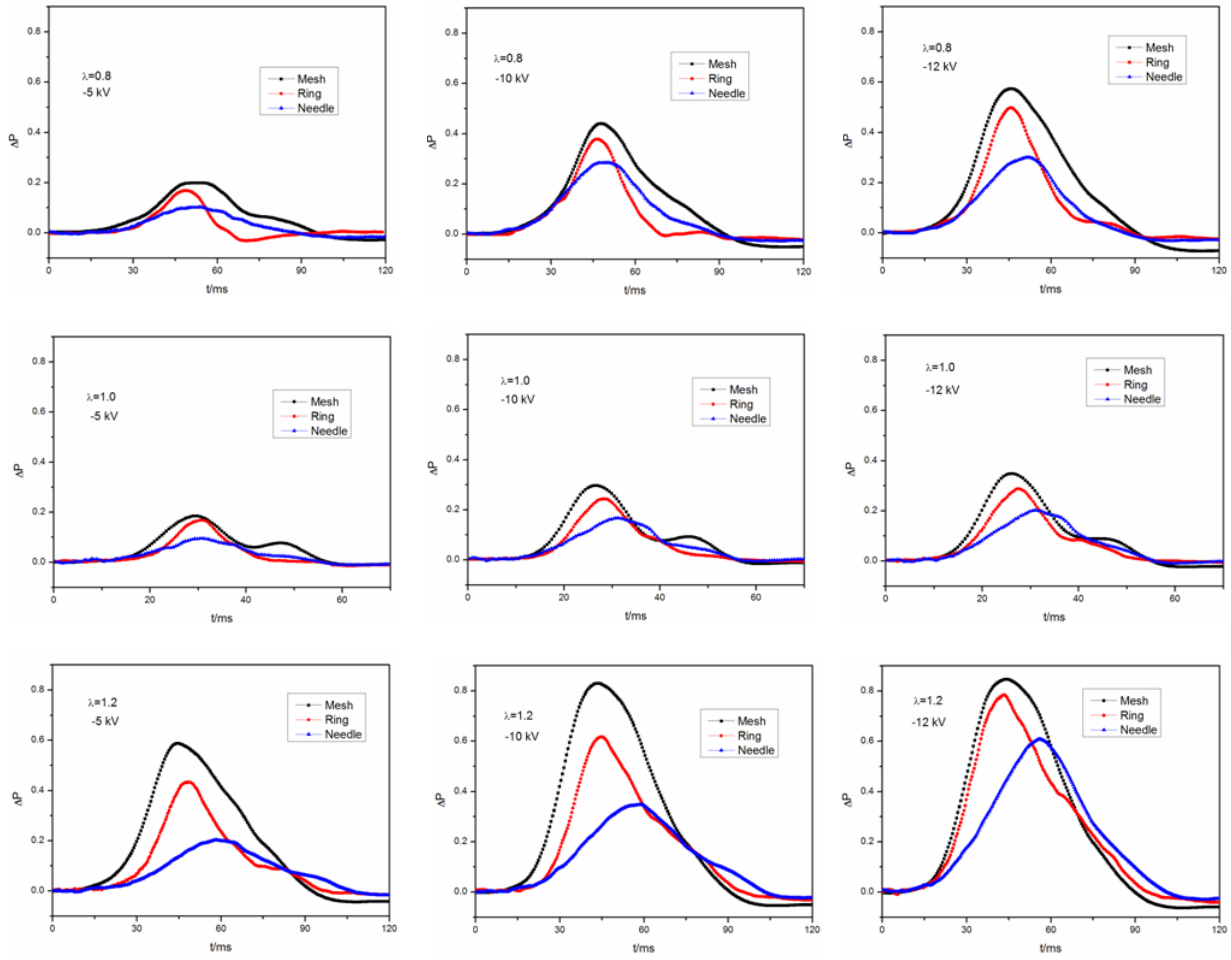

Fig. 11 The rate of the combustion pressure rise for the three electrode geometries

To illustrate directly the effects of the three electrode arrangements on the degree of combustion pressure increase, we define the rate of increase in combustion pressure from the case of no input voltage to the case of a specific input voltage (=u kV) as follows: $\Delta p = \frac{P_u - P_0}{P_0} * 100\%$, where P_u and P_0 are the combustion pressure records for a special electrode at the applied voltages of u and 0 kV, respectively. Figure 11 shows the rate of increase in combustion pressure ΔP under the electric fields generated by the three electrode configurations. It can be seen that when the electric field is applied to the mixture at any excess air ratio, ΔP rises sharply after the short initial stage of combustion, and the peak value of ΔP in the combustion process increases extremely significantly. In the paper, the initial duration (T_{id}) under each condition is explored, which is defined as the time interval from the ignition beginning to the time that $(P_u-P_{init})/P_{init}$ or $(P_0-P_{init})/P_{init}$ reach 5%, where P_{init} is the initial pressure. Additionally, the peak value of the rate of increase in combustion pressure (ΔP_{max}) is obtained from the corresponding curve. The two parameters are used to further evaluate the effects of the three electrode geometries on the pressure variations.

Table 5 The initial duration T_{id} at each excess air ratio under the three electrode geometries (A—mesh, B—ring, C—needle)

λ	0.8			1.0			1.2		
U [kV]	-5	-10	-12	-5	-10	-12	-5	-10	-12
T_{id} for A [ms]	29.5	23.5	21.5	18.9	15.9	14.9	20.5	18.4	17.9
T_{id} for B [ms]	34.6	24.2	23.7	21.5	17.9	16.3	27.6	23.7	18.9
T_{id} for C [ms]	35.2	25.1	24.7	21.9	18.4	17.4	32.3	24.3	20.5

Table 5 shows the initial durations at different excess air ratios for three electrode geometries. It can be seen that the initial duration is reduced in any condition by the applied electric field, and the effect increases with the

[DOI: 10.1299/jtst.2015jtst0020]

increase of the input voltage. For the three electrode geometries, the initial duration for the mesh electrode is the shortest, that for the ring electrode slightly longer and that for the needle electrode the longest. Table 6 shows ΔP_{max} for the three electrode geometries. Obviously, the applied electric field can significantly increase the value of ΔP_{max}, and this effect is enhanced substantially for any electrode geometry with the increase of the input voltage. For the three electrode geometries, the largest ΔP_{max} is presented for the mesh electrode, the second largest value is for the ring electrode, and the last for the needle electrode. For example, at input voltage of -12 kV and lean mixture, ΔP_{max} for the mesh electrode is 84.6%, higher than the ring and the needle electrode by 6.4% and 23.7%, respectively. As for the various excess air ratios, ΔP_{max} at lean mixture is the largest and that for the rich and stoichiometric becomes smaller progressively. It can be seen that for the mesh electrode at -12 kV, ΔP_{max} at lean mixture is 84.6%, higher than the rich mixture and stoichiometric mixture by 33.3% and 49.7%, respectively.

Table 6 The value of ΔP_{max} at each excess air ratio under the three electrode geometries (A—mesh, B—ring, C—needle)

λ	0.8			1.0			1.2		
U [kV]	-5	-10	-12	-5	-10	-12	-5	-10	-12
ΔP_{max} for A [%]	19.9	41	51.3	18.5	29.7	34.9	58.7	83	84.6
ΔP_{max} for B [%]	16.9	37.8	45.8	16.8	24.4	28.8	43.3	61.7	78.2
ΔP_{max} for C [%]	10.3	28.5	30.2	9.7	16.7	20.2	20.2	34.8	60.9

The enhancements of the combustion pressure variations under the applied electric fields are related to the increased flame propagation speed. It is generally accepted that rapid flame speed can enhance the heat and mass interaction between the flame front and the unburned gas mixture. So the initial duration is reduced with increase of the applied voltage. Moreover, the increase of flame speed markedly shortens the overall combustion duration, and induces a reduced heat loss from the flame to the bomb wall. Additionally, the intense wrinkles and distortions appearing in the flame front further enhance the combustion process. As a result, the timing of the maximum pressure at each excess air ratio is all advanced. In the combustion process, the burned gas content within a given period is significantly increased with the flame speed increase, and this induces the peak value of ΔP to increase substantially. The faster the flame propagates than that without electric field, the quicker the combustion process will grow up, which can have even greater influence on combustion pressure variation. As shown in the previous sections, the increase of the flame velocity for the mesh electrode is the biggest, followed by that for the ring and needle electrode. For various excess air ratios, the enhancement of the electric field on the flame propagation velocity at lean mixture is the largest whereas that for the rich and stoichiometric mixture becomes smaller progressively. The increases of the flame speed at each excess air ratio under the three electrode configurations induce the corresponding combustion pressure variations.

Conclusions

1 The electric field distributions developed by the three electrode configurations are all symmetrical, and their direction all point to the high voltage electrodes from the bomb circumference and the vertical bomb centerline. The applied electric fields strongly influence the flame propagation in the horizontal direction rather than in the vertical direction. For the mesh electrode, the electric field strength in the region between the high-voltage electrodes is relatively uniform and its mean value is the largest. While the electric fields for the ring and needle electrodes change relatively large and their mean values decrease progressively.

2 When the electric field is applied, the flame front is stretched remarkably in the direction of the electric field, and the flame propagation velocity is accelerated significantly as the applied voltage increases. In the case of the three electrode geometries, the increase of the flame propagation speed for the mesh electrode is the largest, followed by that for the ring and needle electrode. For various excess air ratios, the increase in the flame propagation speed at lean mixture is the largest, that at rich mixtures the less large and that at stoichiometric mixture the smallest. At the input voltage of -12 kV and lean mixture, the average flame speed for the mesh electrode is increased by 69%, which is higher than that for the ring and the needle electrode by 11%, and 30%, respectively.

3 When the electric field is applied, the combustion pressure growing up is markedly enhanced by the applied electric field, and the timing of peak pressure is advanced with the increase of the input voltage. These behaviors are most pronounced for the mesh electrode, whereas the corresponding influences for the ring and needle electrodes decrease to some degree progressively. For various excess air ratios, the electric field enhances the combustion pressure

[DOI: 10.1299/jtst.2015jtst0020]

variation at lean mixture most significantly, while that for the rich and stoichiometric mixtures decrease progressively in turn. For the lean mixture at the applied voltage of -12 kV, the timing of peak pressure is advanced by almost 23.1% for the mesh electrode, which is higher than that for the ring and needle electrodes about 7.5% and 11.0%, respectively.

Acknowledgements

This study is supported by the National Natural Science Foundation of China (Grants No. 51176150, 51306143 and 51476126). The authors would also express their sincere appreciation to Tsinghua University for its financial support (Grant No. KF14122).

Appendix A. Ionic wind effect

Previous studies on the ionic wind effect have proposed that there exists a collision response time in inducing the ionic wind effect (Min, et al., 2012). The collision response time (t_c) is based on the collision frequency (z) and the ratio of ions to neutral particles (R_i). The ionic wind can be developed by multiple collisions by the ratio of neutral particles to ions ($1/R_i$) multiplied by the characteristic collision time (1/z), resulting in the collision response time $t_c=1/(zR_i)$. For a single ion, there are z collisions per unit time. Among them, the number of collisions with neutrals can be statistically estimated as zn_N/n_t, and the total number of ion-neutral collisions per unit time becomes zn_in_N/n_t, where n_t is number densities of the total particles, n_N is the number densities of neutral molecules before collision, and n_i is the number densities of positive ions. As a consequence, the rate of generation of accelerated neutral molecules (n_N^*) after collision by ions with time (t) is

$$\frac{dn_N^*(t)}{dt} = -\frac{dn_N(t)}{dt} = \frac{n_i n_N(t)}{n_t} z$$

the solutions is

$$n_N^*(t) = n_N(0) \cdot \left[1 - \exp\left(-\frac{n_i}{n_t} zt\right)\right]$$

Since the ratio of number densities of ions to neutrals $R_i = \frac{n_i}{n_N(0)}$ is very small, being of the order of 10^{-8}, so n_i/n_t can be approximated as R_i. By defining the time constant as $t_c=1/(zR_i)$, the number density of accelerated neutral molecules after collision is

$$n_N^*(t) = n_N(0) \cdot \left[1 - \exp\left(-\frac{t}{t_c}\right)\right]$$

References

Altendorfner, F., Kuhl, J., Zigan, L., and Leipertz, A., Study of the influence of electric fields on flames using planar LIF and PIV techniques, Proceedings of the Combustion Institute, Vol.33, No.2 (2011), pp.3195-3201.

Calcote, H.F., and Pease, R.N., Electrical properties of flames-Burner flames in longitudinal electric fields. Industrial and Engineering Chemisitry, Vol.43, No.12 (1951), pp.2726-2731.

Eugene V. Vega, and Ki Yong, Lee, An experimental study on laminar $CH_4/O_2/N_2$ premixed flames under an electric field, Journal of Mechanical Science and Technology, Vol.22, No.2 (2008), pp.312-319.

Gooding, J.M., Bohme, D.K., and Sugden, T.M., Positive ion probe of methane-oxygen combustion, Symposium (International) on Combustion, Vol.16, No.1 (1977), pp.891-902.

Goodings, J.M., Bohme, D.K., and Ng, C.W., Detailed ion chemistry in methane-oxygen flames.1. positive ions, Combust and Flame, Vol.36, No.1 (1979), pp.27-43.

Guo, X.L., Huang, Z.H., Li, Q.Q., and Tang, C.L., Measurements of laminar burning velocities and Markstein lengths of n-butanol-air premixed mixture at elevated temperatures and pressures, Energy &Fuels, Vol.23, No.10 (2009), pp.4900 – 4907.

Huang, Z.H., Wang, Q., Yu, J.R., Zhang, Y., Zeng, K., Miao, H.Y., and Jiang, D.M., Measurement of laminar burning velocity of dimethyl ether-air premixed mixtures, Fuel, Vol.86, No.15 (2007), pp.2360-2366.

[DOI: 10.1299/jtst.2015jtst0020]

Hu, E.J., Huang, Z.H., He, J.J., Jin, C., and Zheng, J.J., Experimental and numerical study on laminar burning characteristics of premixed methane-hydrogen-air flames, International Journal of Hydrogen Energy, Vol.34, No.11 (2009), pp.4876-4888.

Jing Hu., Boris Rivin., and Eran Sher, The effect of an electric field on the shape of co-flowing and candle-type methane-air flames, Experimental Thermal and Fluid Science, Vol.21, No.1-3 (2000), pp.124-133.

Katzer, M., Weber, A.P., and Kasper, G., The effect of electrical fields on growth of titania particles formed in a CH_4-O_2 diffusion flame, Journal of Aerosol Science, Vol.32, No.9 (2001), pp.1045-1067.

Kim, M.K., Ryu, S.K., Won, S.H., and Chung, S.H., Electric fields effect on liftoff and blowoff of nonpremixed laminar jet flames in a coflow, Combustion and Flame, Vol.157, No.1 (2010), pp.17-24.

Kim, M.K., Chung, H.S., and Kim, H.H., Effect of AC electric fields on the stabilization of premixed bunsen flames, Proceedings of the Combustion Institute, Vol.33, No.1 (2011), pp.1137-1144.

Kiyotaka Yamashita., Sunny Karnani., and Derek Dunn-Rankin, Numerical prediction of ion current from a small methane jet flame, Combustion and Flame, Vol.156, No.6 (2009), pp.1227-1233.

Lamoureux, N., Djebaili-Chaumeix, N., and Paillard, C.E., Laminar flame velocity determination for H_2-air-He-CO_2 mixtures using the spherical bomb method, Exp. Therm. Fluid Sci, Vol.27, No.4 (2003), pp.385-393.

Lee, S.M., Park, C.S., Cha, M.S., and Chung, S.H., Effect of electric fields on the liftoff of non-premixed turbulent jet flames, IEEE Trans.Plasma Sci, Vol.33, No.5 (2005), pp.1703-1709.

Marcum, S.D., and Ganguly, B.N., Electric-field-induced flame speed modification, Combustion and Flame, Vol.143, No.1-2 (2005), pp. 27-36.

Memdouh, B., Pascal, D., and Pierre, V., Direct numerical simulation of the effect of an electric field on flame stability, Combustion and Flame, Vol.157, No.12 (2010), pp.2286-2297.

Meng, X.W., Wu, X.M., Kang, C., Tang, A.D., and Gao, Z.Q., Effects of direction-current (DC) electric fields on flame propagation and combustion characteristics of premixed $CH_4/O_2/N_2$ flames, Energy & Fuels, Vol.26, No.11 (2012), pp.6612-6620.

Min Kuk Kim, Suk Ho Chung, and Hwan Ho Kim, Effect of electric fields on the stabilization of premixed laminar Bunsen flames at low AC frequency: Bi-Ionic wing effect, Combustion and Flame, Vol.159, No.3 (2012), pp.1151-1159.

Min Suk Cha., Member IEEE., and Yonggyu Lee., Premixed combustion under electric field in a constant volume chamber, IEEE Trans. Plasma Sci, Vol.40, No.12 (2012), pp.3131-3138.

Papac, M.J., and DUNN-RANKIN, D., Modelling electric field driven convection in small combustion plasmas and surrounding gases, Combustion Theory and Modelling, Vol.12,No.1 (2008), pp.23-44.

Ryu, S.K., Kim, Y.K., Kim, M.K., Won, S.H., and Chung, S.H., Observation of multi-scale oscillation of laminar lifted flames with low-frequency Ac electric fields, Combustion and Flame, Vol.157, No.1 (2010), pp.25-32.

Sakhrieh, A., Lins, G., Dinkelacker, F., Hammer, T., Leipertz, A., and Branston, D.W., The influence of pressure on the control of premixed turbulent flames using an electric field, Combustion and Flame, Vol.143, No.3 (2005), pp.313-322.

Shinichi Moriya, Koji Yoshida, Hideo Shoji, and Akira Iijima, The effect of uniform and non-uniform electric fields on flame propagation, Journal of Thermal Science and Technology, Vol.3, No.2 (2008), pp.254-265.

van den Boom, J.D.B.J., Konnov, A.A., Verhasselt, A.M.H.H., Kornilov, V.N., de Goey, L.P.H, and Nijmeijer, H., The effect of a DC electric field on the laminar burning velocity of premixed methane/air flames, Proceedings of the Combustion Institute, Vol.32, No.1 (2009), pp.1237 – 1244.

Volkov, E. N., Kornilov, V. N., and de Coey, L. P. H., Experimental evaluation of DC electric field effect on the thermoacoustic behavior of flat premixed flames, Proceedings of the Combustion Institute, Vol.34, No.1 (2013), pp.955-962.

Wisman, D.L., Marcum, S.D., and Ganguly, B.N., Electrical control of the thermodiffusive instability in premixed propane-air flames, Combustion and Flame, Vol.151, No.4 (2007), pp.639-648.

[DOI: 10.1299/jtst.2015jtst0020]

Won, S.H., Cha, M.S., Park, C.S., and Chung, S.H., Effect of electric fields on reattachment and propagation speed of tribrachial flames in laminar coflow jets, Proceedings of the Combustion Institute, Vol.31, No.1 (2007), pp.963-970.

Won, S.H., Ryu, S.K., Kim, M.K., Cha, M.S., and Chung, S.H., Effect of electric fields on the propagation speed of tribrachial flames in coflow jets, Combustion and Flame, Vol.152, No.4 (2008), pp.496-506.

Xie, L., Kishi, T., and Kono, M., The influence of electric fields on soot formation and flame structure of diffusion flames, Journal of Thermal Science, Vol.2, No.4 (1993), pp.288-293.

Zake, M., Barmina, I., and Turlajs, D., Electric field control of polluting emissions from a propane flame, Global Next: the Int. J, Vol.3, No.2 (2001), pp.95-108.

[DOI: 10.1299/jtst.2015jtst0020]